Integrating CAD and Nano-Indentation for Complex Lithograph

Kangmin Xu
Seung-Cheol Yang
Xiaoping Qian*
Mechanical, Materials and Aerospace Engineering Department
Illinois Institute of Technology
Chicago, IL 60062, USA

ABSTRACT

We present an approach for producing complex nanoscale patterns by integrating computer-aided design (CAD) geometry processing with an atomic force microscope (AFM) based nanoindentation process. Surface modification is achieved by successive nano-indentation using a vibrating tip. By incorporating CAD geometry, this approach provides enhanced design and patterning capability for producing geometric features of both straight lines and freeform B-splines. This method automatically converts a pattern created in CAD software into a lithography plan for successive nanoindentation. For ensuring reliable lithography, key machining parameters including the interval of nanoindentation and the depth of nanogrooves have been investigated, and a proper procedure for determining the parameters has been provided. Finally, the automated nanolithography has been demonstrated on poly methylmethacrylate (PMMA) samples. It shows the robustness of complex pattern fabrication via the CAD integrated, AFM based nanoindentation approach.

1 Introduction

During the last decade, atomic force microscope (AFM) based mechanical nanolithography has been often used in fabricating various nanostructures such as protein biosensors [1], single electron transistors [2], and Coulomb blockades [3]. An AFM based nanolithography process typically uses direct mechanical scratching via its tip to remove material. Alternative methods also include chemical oxidation or other physical processes [4]. The key advantages of such AFM based lithographic processes are their capability of producing and modifying nanoscale patterns with low cost, high spatial resolution, and in ambient environment [5] [6]; AFM lithography allows direct pattern modification without any additional processes. It is capable of achieving features with size less than 10 nm. Further, AFM based lithography enables in-situ lithography and measurement [7]. In order to improve the lithography efficiency and pattern quality and further to automate the process, this paper proposes the integration of CAD geometry processing with a nanoindentation based lithography process for producing complex pattern.

Although this concept of integrating CAD systems in a nanolithography system [8] [9] [10] , including the integration of CAD with static [11] [12] [13] [14] and dynamic plowing techniques [7] [10] [15], has been suggested in the literature, thus far, only limited geometry such as circles and straight lines are fed into nanolithography systems. For example, the automated lithography based on static and dynamic lithography is only available with simple patterns composed of dots and lines. In addition, they still have difficulties in controlling precise tip movement for complex pattern fabrication. Static plowing lithography is performed in the contact mode to cut a groove on the sample surface with a sharp tip. However, it was shown that irregular shapes in the edge of the profile could arise during the process due to the twisting of the cantilever and stick-slip motion of the tip [16]. Therefore, pattern geometry could be affected by weak plowing around a certain angle to the cantilever axis [10] [6]. In dynamic plowing lithography (DPL), a vibrating tip is utilized in the tapping mode to plough the sample surface. Since the vibrating tip is less affected by the dragging force during the process, it can alleviate the difficulty of cantilever distortion [10]. However, it was shown that DPL makes a deep hole early in the process of dynamic plowing,

*Correspondence can be sent via email to qian@iit.edu.

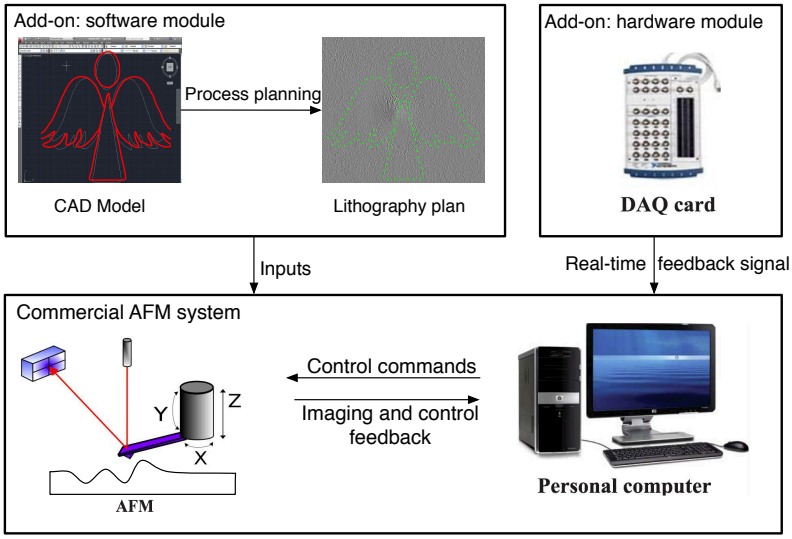

Fig. 1. Overview of the nano lithography system

but makes small indentations late in the process [7]. As a result, DPL may lead to inconsistent plowing in machining line structures.

In this paper, we present a novel nanoindentation method that enables automated fabrication of complex patterns via nanoindentation. A nanoindentation technique creates a nanohole on the surface at a specified location, which leads to contact in a vertical direction one at a moment. By avoiding lateral tip motions during the process, the technique can produce a regular hole shape without any directional restrictions [17]. For simple pattern fabrication, some researchers have already proved that nanoindentation can be used to draw a solid line by a sequence of overlapped nano-holes [18] [19]. In spite of this advantage, little work has been done with regard to the automation of nanoindentation technique. In this paper, we focused on extending the patterning capability of nanoindentation for complex pattern fabrication. The proposed method enables realization of patterns of precise CAD features such as straight lines and freeform B-spline geometry, providing the automated lithography for arbitrary pattern fabrication without user intervention. In addition, the key machining parameters for extending the nanoindentation to a lithography process, such as interval distance and indentation depth, have been studied in order to ensure high reliability in the patterning process.

In the remainder of this paper, the experimental setup and the point-based nano-lithography method are introduced in Section overview of the system and point-based lithography. CAD guided process planning of 2D patterns is introduced in Section CAD guided process planning. In Section results and discussion, we present the results from integrating the point-based method with the automatically generated path from a CAD model. Finally the paper is concluded in Section conclusion.

2 Overview of the system

The automated lithography system is constructed based on a commercial AFM platform shown in Fig. 1. The AFM system consists of an AFM (5500 Atomic Force Microscope, Agilent Technology Inc.), a data-acquisition (DAQ) card (NI USB 6229 BNC, National Instruments) and a PC. The microscope, head electronics box, AC controller, and PicoScan controller constitute the AFM system. The signal access module, voltage divider, DAQ card and the computer are installed for the real-time data acquisition system. The piezoelectric scanners have an xy scan range of 90 μm and a z scan range of 200nm.

For the automated process plan generation, we have developed a software module to convert complex patterns from CAD systems into a lithography plan using the Agilent's Application Program Interface (API) scripts. A pattern is designed in commercial CAD software and transferred as CAD data formats of IGES and DXF to a home-built CAD model interpreter. Our CAD model interpreter is able to convert the CAD file into a set of the API of the commercial AFM system to represent a lithography plan. The method thus enables the automated process planning for complex pattern fabrication with CAD geometric features.

The automated nanolithography method utilizes the vibrating tip of the AFM in the tapping mode. A diamond-like carbon (DLC) coated tip with high stiffness is employed for surface modification, and its radius is approximately 15nm. The sample is prepared with poly methylmethacrylate (PMMA) of a thickness of 90 nm on the silicon substrate. Surface modification is achieved through a vibrating tip at near resonance frequency of 200$\sim$400 kHz. Since the tip is compatible for image scanning and nanolithography, in situ imaging is possible. The algorithm for automated nanolithography is programmed us-

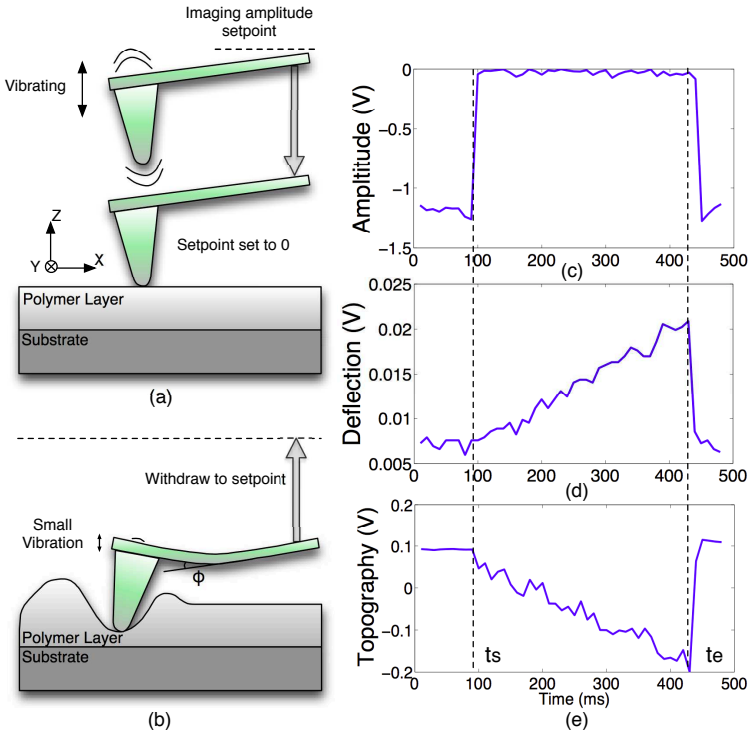

Fig. 2. Process of the point-based lithography (a) Approaching and Contacting (b) Indenting and Withdrawing (c) Amplitude signal during nanoindentation (d) Deflection signal during nanoindentation (e) Topography signal during nanoindentation

ing the API provided by the commercial AFM system, which facilitates a set of controls for tip positioning, setpoint control, and DAQ access for real time data acquisition. The tip position is controlled by a feedback system of piezoscanners.

3 Point-based lithography

In this section, we describe our nanoindentation process which essentially is a point-based lithography process. We then describe how we determine the key process parameters. To automate the nanolithography process, a point-based lithography process has been developed by combining a novel nanoindentation technique with CAD geometry processing. The point-based lithography aims to carve nano-grooves by indenting successive nano-holes along a CAD pattern design. In contrast to plowing techniques that carve patterns with lateral tip motion, this method confines surface modification to nanoindentation at a stationary point in order to minimize the lateral force exerting on the tip. This allows precise tip control to fabricate a complex pattern without any directional restrictions. In addition, point-based lithography involves an automated lithography plan using a process plan that interprets a pattern designed in CAD software to fabricate a sequence of nano-indentation.

3.1 Methodology of nanoindentation

Nanoindentation is a mechanical lithography process to indent a single hole using a sharp tip while the cantilever is stationary at a specific point. When extending nanoindentation to lithography, i.e. point-based lithography, this method applies normal contact force to the vibrating tip in the tapping mode to deform surface structure. When the tip is operated in the tapping mode, the cantilever is vibrated by a dither piezo; the cantilever amplitude is monitored and stabilized by a feedback system. The feedback system aims to keep a specific amplitude value (setpoint) during the process by controlling the distance between the tip and the sample. Since the amplitude is changed with respect to the distance between tip and sample, the topography of the surface is obtained by the difference between the setpoint and the change of amplitude corresponding to surface topography. For image scanning in the tapping mode, the setpoint is decided such that the tip is slightly touching the surface without indentation.

In point-based lithography, the setpoint is adjusted into zero to achieve nanoindentation. Once the process is triggered by changing the setpoint value to zero as shown in Fig. 2a, the tip is moved close to the sample by feedback loop. As a result, the tip oscillation is attenuated significantly due to tip-sample interaction. However, the amplitude is still above zero because dither piezo keep vibrating the tip. By decreasing the difference between the zero setpoint and the current amplitude, the tip is continuously pushed down to the surface by the feedback system as shown in Fig. 2b. This process induces plastic deformation of the surface until the deflection of cantilever reaches a threshold value. When the tip deflection reaches a

threshold value, a setpoint is reset to image scanning amplitude as shown in Fig. 2b. and the tip is lifted away from the sample.

The detailed AFM operation can be verified by observing the signals in Fig. 2c-e, which show the change of amplitude and the deflection from the cantilever bending during the process. By changing the setpoint to zero, the feedback system drives the z piezoelectric actuator down to dampen the amplitude to zero at the time t_s. The deflection signal, representing the bending of the cantilever, begins increasing with the change of topography. During the process, indentations occur between tip and sample. As shown in Fig. 2e, the feedback system keeps lowering the tip until the deflection signal reaches the threshold value at the time of t_e.

3.2 Parameters for point-based lithography

Based on the nanoindentation technique, point-based lithography extends the lithographic capabilities by overlapping successive nano-holes. A chain of nano-holes forms a continuous lines and curves to fabricate a complex pattern by selecting the interval between successive nano-holes, the depth of nano-grooves, and waiting times for settling tip position. Since the result of parameter settings depends on the geometry and the material of the tip, thickness and hardness of the sample material, and cantilever stiffness, each parameter needs to be investigated properly for a particular system setting.

3.2.1 Interval determination

In order to fabricate continuous features, the interval of overlapped nano-holes is the most significant parameter. Since the interval (interval I) is limited by hole radius and bulge effect of nanoindentation as shown in Fig. 3a, a set of nanoindentation experiments have been performed to evaluate the hole size with respect to deflection threshold. The hole shape is generally asymmetric and the size of bulge is different around the hole because the tip shape is not typically symmetric. Therefore, the resulting hole radius R is measured as a minimum radius in the hole profile. Fig. 3b shows corresponding hole radius to various deflection thresholds and a quadratic polynomial is fitted to represent the relationship. For small deflection thresholds, the hole radius is measured about 11 nm, which represents the size of the sharp tip radius r_{tip} ($\sim 15nm$) with small indentation. However, with rising deflection thresholds, the hole radius shows a dependency with the defleciton threshold. In addition, the deflection threshold above $0.045V$ shows that the increasing rate of hole radius slowed down. This is because the bending of the cantilever accumulates large bulge and indents the longer hole radius in the cantilever direction during the indentation. In addition, a threshold above 0.055 V tends to break the tip after several tens of the nanoindentation process. This dependency is utilized to determine the interval to fabricate continuous lines.

Fig. 4 shows the effect of the hole interval on the horizontal direction in indenting a solid line. For the interval with $0.5R$, R, and $2R$, nanogrooves have been machined with the deflection threshold of $0.02V$ and the corresponding hole radius of $20nm$. As can be seen from this figure, with the increase of interval I from 0.5R to 2R, the depth of nanogroove becomes smaller and smaller. With the interval of 0.5R, the tip makes initial contact at a lower point from the surface, which decreases the amount of residual bulge staying in the nanogroove and allows indenting a deeper groove with a given tip normal force. With the interval of 2R, there exists a rough and shallow nanogroove due to poor overlapping between successive nanoindentations where the bulge resulted from one indentation is not fully indented by subsequent indentation . The subsequent nanoindentation shifts the bulged materials backward to fill the bottom of the formed nanogroove. As a result, the height profile becomes shallow. When the interval $I \leq R$, the resulting groove tends to have substantial, uniform depth. For time efficiency of nano indentation, it is unnecessary to consider $I < R$ since the interval of R can create nanogrooves with consistent height profile and the least number of holes to be indented. Therefore, the resulting $I = R$ is used in further experiments for lines with all lines and curves. In point-based lithography, the standard spacing for nanogrooves is determined as the minimum hole radius to the deflection threshold.

3.2.2 Depth control

The essential parameter to control depth of nanogrooves is the deflection threshold for nanoindentation. With the interval of hole radius R, the deflection value determines the depth of the nanogrooves. In order to characterize the dependency of the deflection threshold, a set of nanogrooves have been fabricated with increasing deflection thresholds. Fig. 5 shows the depth of 9 lines that is machined with increasing deflection thresholds, ranging from 0.005 V to 0.055 V with the corresponding interval as discussed in the previous section. The depth of each line is obtained by measuring 20 random points along the nanogroove. The resulting curve in Fig. 5 increases with the deflection value. However, the depth with a high deflection threshold leads to the bending of the cantilever. It brings about the lateral translation of the tip along the cantilever axis. This result causes the slope of the curve to drop. This is interesting phenomenon that reveals a limitation of a single nanoindentation process to surface modification. In addition, the curve shows the effective deflection threshold to control the depth for nanogrooves. The approximate depth of nano-grooves can be selected on the deflection to depth curve. To investigate depth profile of a nanogroove with respect to machining directions, 4 nano-grooves have been demonstrated with various machining directions. The depth profile of each groove is shown in Fig. 6. Although the depth profiles are not

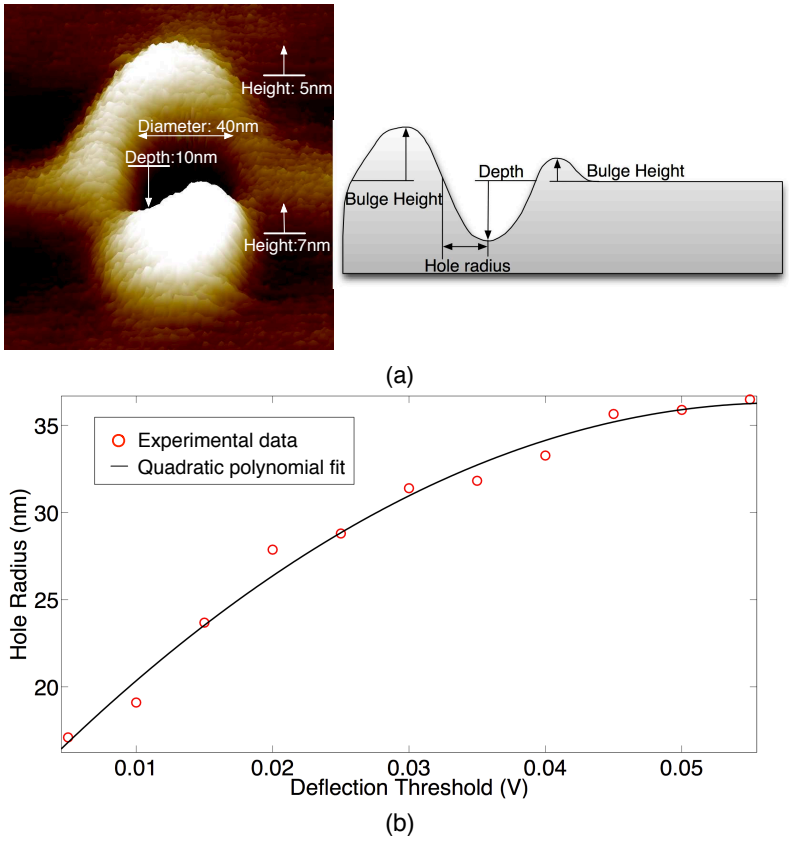

Fig. 3. (a)3D AFM image of a single hole fabricated by nano indentation process and (b)Dependence of the hole radius to deflection threshold

identical, each groove was machined with a consistent depth profile with deflection threshold of $0.02V$ in any machining direction. The depth of the grooves was machined without a restriction of machining directions. For the nano-groove in the pattern, the average depth was measured as 17.3 nm with standard deviation 4.9 nm and the average width of the groove was 48.5nm with standard deviation 3.4 nm.

3.2.3 Time interval determination

During successive nanoindentation, the tip iterates vertical indentation and lateral transition in sequence. Between two distinct motions, two pause times needs to be set to allow system settlement for both before indentation t_{p1} and after indentation t_{p2}. The two pause times ensure that the tip stops at the right position when the tip is placed and avoids undesired

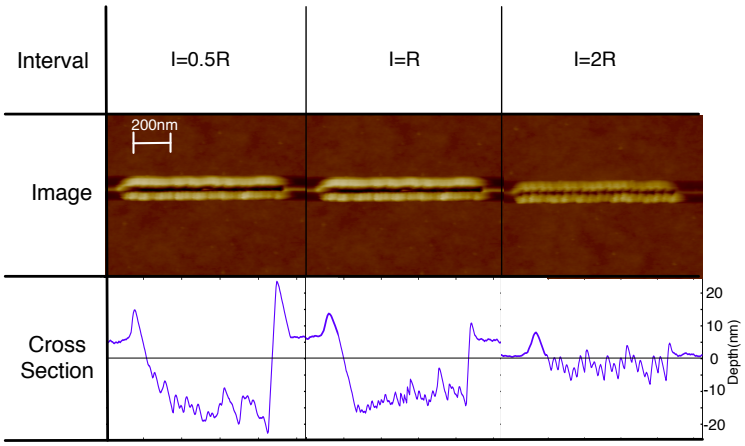

Fig. 4. Line fabrication with the interval of $0.5R$, R, and $2R$ and height profiles along the lines

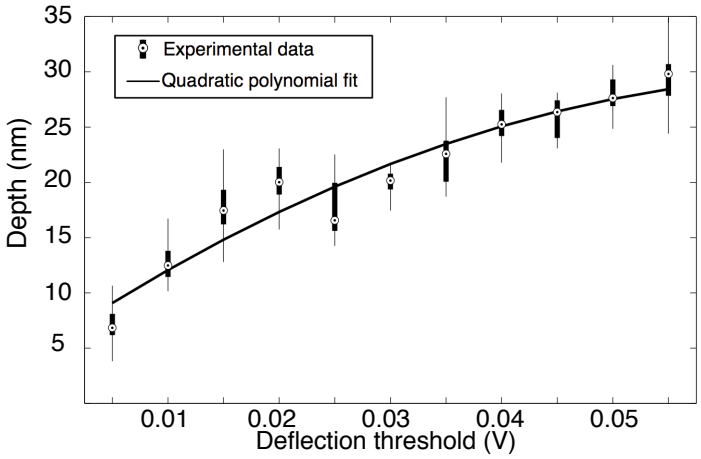

Fig. 5. Line depths for 20 random points of each line according to the deflection threshold from 0.005 V to 0.055 V

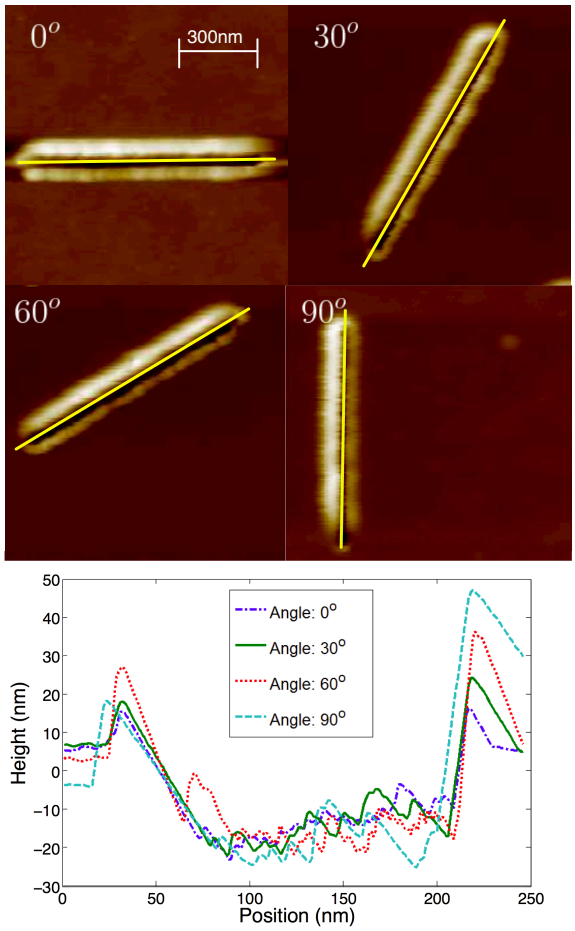

Fig. 6. AFM image and the depth profile of each nano-groove

scratching when the tip is retreated. The time of t_{p1} involves tip travel time between each indentation and response time for a closed loop system. The tip travel time is estimated with respect to tip velocity and travel distance, and the response time for the closed loop system is measured by observing the output voltage of X-Y piezoelectric actuators and Z piezoelectric actuator though a DAQ card. Each piezoelectric actuator needs settling time such that the closed loop system compensates nonlinearity of tip motion. Fig. 7 shows the transient response of closed loop system for X piezo and Z piezo during the tip travel. By observing the response delay of the output voltage, we assigned $0.1s$ for the time t_{p1} and a minimum time of $0.06s$ for the time t_{p2} for full tip withdrawal. The time t_{p2} involves tip travel time in Z direction and a settling time. With

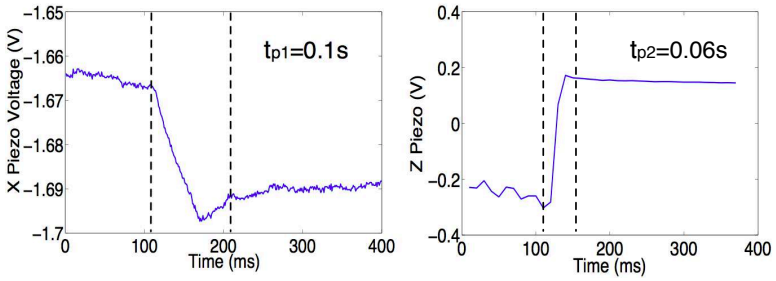

Fig. 7. Pause time for both before indentation t_{p1} in X-Y piezo and after indentation t_{p2} in Z piezo

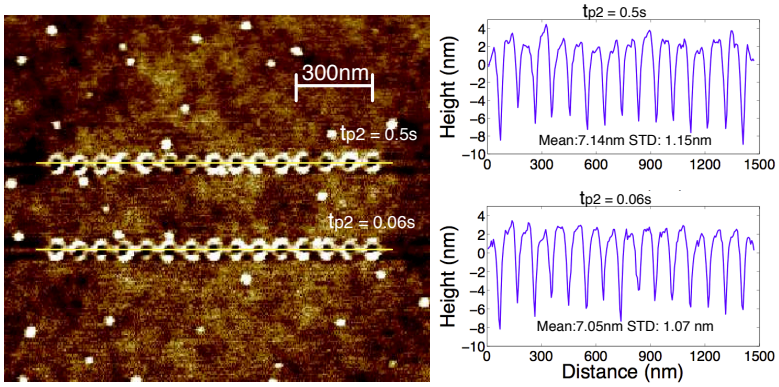

Fig. 8. Pause time after nanoindentation to guarantee tip withdraw

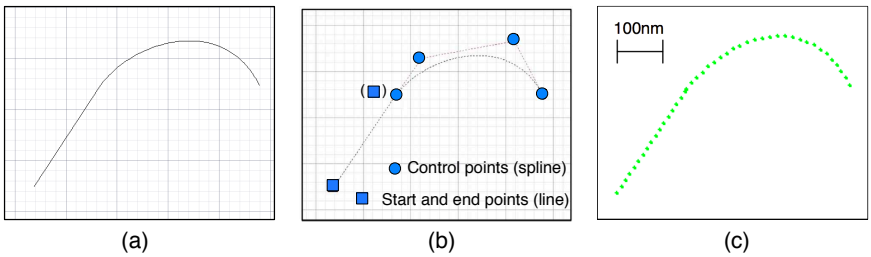

Fig. 9. Typical CAD model of a line and a curve (a) Drawing; (b) Generating points from lines and B-spline curves; (c) indentation points generation

the minimum withdrawal time of $0.06s$, the hole depth and shape can be achieved consistently without additional damage on the surface as shown in Fig. 8. In a case of the nanoindentation process with deflection value $0.02\ V$, the total time for indenting a single hole is estimated around $0.83s$. Indenting a nano-hole takes about $0.64s$ to modify sample surface and locating the tip at a new position takes around $0.002ms$ with the tip velocity of $45\mu m/s$. The time of $0.015s$ is taken to control the signal by way of the DAQ card. Since the total time for nanoindentation is varied by the hole depth, the time for surface modification can be different with respect to the deflection threshold.

4 CAD guided process planning

For automation of the point-based method, we have developed a CAD guided process planning module that is capable of generating automatically a lithography plan by incorporating CAD geometry. In the point-based method, a series of points need to be distributed uniformly on the pattern design with the corresponding interval length. The interval length is pre-determined for the sake of depth control. As shown in Fig. 3 and Fig. 5, line depth determines the effective deflection threshold and the associated hole radius so that the interval length is accordingly determined as the minimum hole radius. The CAD geometry information facilitates the conversion of complex patterns into a point array for tip lateral motion. Fig. 9 show the schematic procedure for CAD guided process planning. First, a pattern design is created and edited in a CAD system (Fig. 9a). The CAD model consisting of lines and B-splines (Fig. 9b) is converted into point arrays for a lithography plan (Fig. 9c).

The point array for lateral tip motion is derived from two algorithms to interpret pattern models with B-splines and lines. For curve shape fabrication, each point are determined by using an analytic representation of B-splines; B-splines is the de factor standard representation of freeform geometry in the CAD systems. The general form of the B-spline curve is given as

$$C(t) = \sum_{i=0}^{n} P_i N_{i,p}(t) \tag{1}$$

where P_i are the control points, n is the number of control points, $N_{i,p}(t)$ are the p-th degree B-spline basis functions and are defined recursively using knot vector $T = t_0, t_1, ..., t_m$; m is the number of knots and the degree $p = m - n - 1$. With the information above, the basis function is defined as

$$N_{i,0}(t) = \begin{cases} 1, & if \;\; t_i \leq t < t_{i+1} \;\; and \;\; t_i < t_{i+1}; \\ 0, & otherwise. \end{cases} \tag{2}$$

$$N_{i,j}(t) = \frac{t - t_i}{t_{i+j} - t_i} N_{i,j-1}(t) + \frac{t_{i+j+1} - t}{t_{i+j+1} - t_{i+1}} N_{i+1,j-1}(t) \tag{3}$$

where $j = 1, 2, ..., p$. By using Cox-de Boor algorithm, only the control points that affect the point will be considered. The Cox-de Boor algorithm [20] is given as

$$P_i^j(t) = (1 - \alpha_i^j) P_i^{j-1}(t) + \alpha_i^j P_{i+1}^{j-1}(t) \tag{4}$$

where

$$\alpha_i^j = \frac{t - t_{r-j+i}}{t_{r+i} - t_{r-j+i}} \tag{5}$$

for $j = 1, 2, ..., p$ and $i = 0, 1, ..., p - j$. i, j shows the layer computing layer and sequence of each layer in the Cox-de Boor algorithm. The parameter t is in the interval $t \in [t_r, t_{r+1})$. Symbols r, p, j, P_i^0, P_i^j, P_0^p denote the index of knot interval, the degree of B-spline curve, the index of computing layer of the Cox-de Boor algorithm, the control point same as Pc_i, the de Boor point and the final interpolation point, respectively. Point locations on the curve have been found in a variation of t; the value of t is explored to meet the requirement that the distance between these two points is equal to the interval I as

$$|P_0^j(t_{n+1}) - P_0^j(t_n)| = I \tag{6}$$

where $n = 0, 1, ...,$, t_{n+1} and t_n are parameters meeting the requirement and initially $t_0 = 0$. Recursively, t_n and related $P_0^j(t_n)$ can be found. Points $P_0^j(t_n)$ meeting the requirement are saved as Pm_i for machining. Repeatedly, all points with constant interval I can be obtained on the curve. Fig. 10 shows desired points on the surface.

Point locations on the line are evaluated with a unit line vector and the point interval. Each line is described by a pair of start point P_s and end point P_e. Subsequently, a unit vector of each line can be obtained as

$$\vec{V} = \frac{Pe - Ps}{|Pe - Ps|} \tag{7}$$

Starting from the start point P_s, the machining points can be found as

$$Pm_i = P_s + I \times i \times \vec{V} \tag{8}$$

where i is integer and $i \in [0, \frac{|Pe-Ps|}{I}]$.

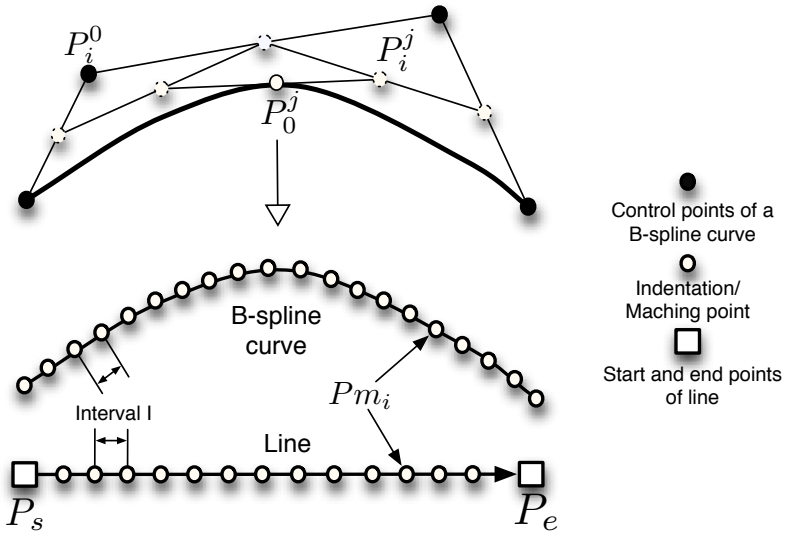

Fig. 10. B-spline curve representation using the Cox-de Boor algorithm

Algorithm 1 Automated nano lithography

Import the CAD models (lines and curves)
Setting entity counter m, including both lines and curves
for $i = 1 \rightarrow m$ **do**
  if entity=line ("110" in IGES, "AcDbLine" in DXF) **then**
    Get start point and end point of current line Ps_i and Pe_i
    Get unit vector $\vec{V} = \frac{Pe_i - Ps_i}{|Pe_i - Ps_i|}$
    From start point, with interval I to get points Pm_i on the line until end point
    Use point-based lithography to machine the points Pm_i with parameters (deflection threshold, t_{p1}, t_{p2})
  else
    if entity=spline ("126" in IGES, "AcDbSpline" in DXF) **then**
      Get control points, knot vector, degree
      Using cox-de Boor, start from the first control point, find the next neighbor points $P_0^j t_n$ on the curve with interval I until the end point
      Use point-based lithography to machine the points Pm_i with parameters (deflection threshold, t_{p1}, t_{p2})
    end if
  end if
end for
Scan the save the images as machining results

4.1 Automated lithography algorithm

The AFM tip is located along a lithography plan generated from the CAD guided process planning module and makes a series of nanoholes with predefined parameters. Algorithm I describes the automated scheme for CAD guided process planning and nanoindentation technique. The process plan is created based on a pattern designed in a CAD environment. The geometric information (control points, degree, knot vector, etc.) of the B-spline curves and lines are extracted from CAD files (for example, IGES and DXF files) and interpreted into indenting points in vector scan mode. With the process plan, point-based lithography executes serially nanoindentation and lateral tip transition. The tip motion is planned and implemented with the API scripts of commercial AFM, which interprets the information of CAD geometric entities into the lithography path. Additional waiting time is imposed to allow for system settling down: pause time before indentation t_{p1} and pause time after indentation t_{p2}; they are predetermined based on the response delay of piezoelectric actuators. The depth of the pattern is indicated by cantilever deflection as shown in Fig. 5. Once the whole nano indentation process is completed, a full image scan in tapping mode is immediately invoked to obtain the result of indentation without changing the tip.

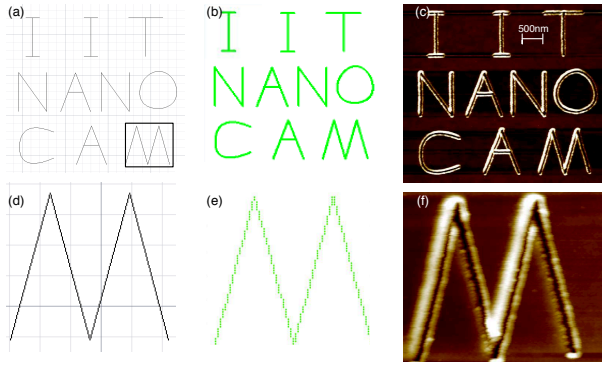

Fig. 11. “IIT NANO CAM” fabricated by point-based lithography (a) Drawing in AutoCAD (b) Topography image (c) Path generation (d) Lithography plan for a letter ’M’

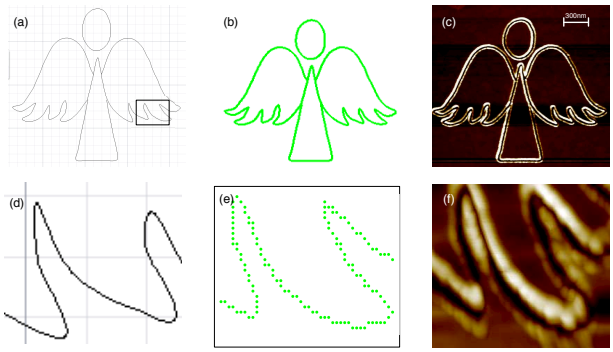

Fig. 12. Continuous angel pattern (a) Drawing in AutoCAD (b) Lithography plan for wing part (c) Topography image (d) Cross section of wing part

5 Results and discussion

In order to investigate the capability of the point-based lithography, we have fabricated an “IIT NANO CAM” pattern on a PMMA substrate of a thickness of 90 *nm* on the silicon substrate. The nanolithography experiment was performed in the tapping mode with a diamond coated tip cantilever with a spring constant of $40N/m$. In order to minimize the effect of nonlinearity of the piezoelectric actuator, we have used a closed loop feed back system. The pattern was designed and modified using commercial CAD software as shown in Fig 11.a. The letter ’O’ and ’C’ was designed with B-splines and other letters were written with lines. The CAD guided process planning module we developed for point-based lithography converts the pattern design into a lithography plan. Fig 11.b shows the nanoindentation path that composed of a set of overlapped points derived from each letter in the scanning range of $5\mu m \times 5\mu m$. The total number of indenting points used in the pattern was 1134 and the total machining time was about $758s$. Between each indenting point, waiting time was set $0.06s$ and the length of interval was $27nm$ with a deflection threshold of $0.02V$. In this pattern, the results shows that the nanogrooves was successfully created without directional restrictions and the effect from asymmetric hole and bulge shape was reduced with the given interval. The depth of nanogrooves is measured by AFM profiles at different points on the pattern. The average depth is $17.8nm$ and it shows the homogeneity of the nanogroove depth. This indicates that the relation between deflection threshold and depth is consistent and confirmed during the lithography process.

In addition, we show a second example where complex patterns of an angel shape containing a set of B-spline curves as shown in Fig 12 has been produced. The angel pattern involved indenting 1058 points and the total machining time is about $656s$. The deflection threshold was set $0.02V$ for the average depth of $18.9nm$. The interval between each hole was at 27 *nm*. Although there was bulge along either side of grooves, the shapes of the B-spline curves at the corners were machined without any discernible discontinuity as shown in Fig 12c and d.

6 Conclusion

This paper extends a point-based nano indentation process into a nano lithography process. It further integrates the lithography process with CAD geometry processing for automatically producing complex nanoscale patterns. Machining parameters for the point-based lithography, such as deflection threshold and pause times, were defined by experiments with the pattern topography and nanoindentation parameters. We have successfully fabricated complex patterns composed of

multiple B-splines curves. This method shows the capability of complex pattern fabrication without user intervention during the lithography process. The analysis of nano-groove depth shows the consistent removal rate without any restriction of machining direction has been obtained during the process.

The integration with CAD software has broadened the pattern complexity and improved the automation level of the lithography system. A script interpreter developed for the point-based method enables the automation of complex pattern fabrication. The point-based lithography currently allows patterns to be fabricated within a maximum range of AFM scanners ($90\mu m \times 90\mu m$) in a single process. To extend the potential application domain size, the entire pattern needs to be partitioned and fabricated in multiple processes and the precise positioning of the AFM scanners is needed.

The minimum line width of patterns is determined by a single hole radius. An increase in line width is possible by increasing the deflection threshold, with larger tips or overlapping indentation paths. Although z-axis piezoelectric actuating speed can be increased and larger radius tips (thus larger indentation intervals between successive indentation points) can be used to improve the indentation efficiency, this point-based lithography process is still a serial process. Its throughput can be significantly improved by using parallel indentation with multiple tips.

Achnowledgements

The authors gratefully acknowledge the financial support from the Nation Science Foundation grants #0800912 and CNS#1035844.

References

[1] Garno, J. N., and C., J., 2008. "Afm-based lithography for nanoscale protein assays". *Analytical Chemistry,* ***80***(5), pp. 1361–1369.

[2] Schumacher, H., Keyser, U., Zeitler, U., Haug, R., and Eberl, K., 2000. "Controlled mechanical afm machining of two-dimensional electron systems: fabrication of a single-electron transistor". *Physica E: Low-dimensional Systems and Nanostructures,* ***6***(1-4), pp. 860–863.

[3] Do, Q. T., Clemens, H., and Lorke, A., 2003. "Coulomb blockade systems fabricated by atomic force microscopy". In Nanotechnology, 2003. IEEE-NANO 2003. 2003 Third IEEE Conference on, Vol. 2, pp. 774 – 777 vol. 2.

[4] Tseng, A. A., Notargiacomo, A., and Chen, T. P., 2005. "Nanofabrication by scanning probe microscope lithography: A review". *Journal of Vacuum Science & Technology B*.

[5] Binnig, G., Quate, C. F., and Gerber, C., 1986. "Atomic force microscope". *Phys. Rev. Lett.,* ***56***(9), Mar, pp. 930–933.

[6] Jung, T., Moser, A., Hug, H., Brodbeck, D., Hofer, R., Hidber, H., and Schwarz, U., 1992. "The atomic force microscope used as a powerful tool for machining surfaces". *Ultramicroscopy,* ***42***, pp. 1446–1451.

[7] Heyde, M., Rademann, K., Cappella, B., Geuss, M., Sturm, H., Spangenberg, T., and Niehus, H., 2001. "Dynamic plowing nanolithography on polymethylmethacrylate using an atomic force microscope". *Review of Scientific Instruments,* ***72***, p. 136.

[8] Johannes, M., Kuniholm, J., Cole, D., and Clark, R., 2006. "Automated cad/cam-based nanolithography using a custom atomic force microscope". *Automation Science and Engineering, IEEE Transactions on,* ***3***(3), pp. 236–239.

[9] Johannes, M., Cole, D., and Clark, R., 2007. "Three-dimensional design and replication of silicon oxide nanostructures using an atomic force microscope". *Nanotechnology,* ***18***, p. 345304.

[10] Klehn, B., and Kunze, U., 1999. "Nanolithography with an atomic force microscope by means of vector-scan controlled dynamic plowing". *Journal of applied physics,* ***85***, p. 3897.

[11] Wendel, M., Kuhn, S., Lorenz, H., Kotthaus, J., and Holland, M., 1994. "Nanolithography with an atomic force microscope for integrated fabrication of quantum electronic devices". *Applied physics letters,* ***65***(14), pp. 1775–1777.

[12] Oesterschulze, E., Malave, A., Keyser, U., Paesler, M., and Haug, R., 2002. "Diamond cantilever with integrated tip for nanomachining". *Diamond and Related materials,* ***11***(3-6), pp. 667–671.

[13] Fang, T., and Chang, W., 2003. "Effects of afm-based nanomachining process on aluminum surface". *Journal of Physics and Chemistry of Solids,* ***64***(6), pp. 913–918.

[14] Schumacher, H., Keyser, U., Zeitler, U., Haug, R., and Eberl, K., 1999. "Nanomachining of mesoscopic electronic devices using an atomic force microscope". *Applied physics letters,* ***75***, p. 1107.

[15] Cappella, B., and Sturm, H., 2002. "Comparison between dynamic plowing lithography and nanoindentation methods". *Journal of applied physics,* ***91***, p. 506.

[16] Bouchiat, V., and Esteve, D., 1996. "Lift-off lithography using an atomic force microscope". *Applied physics letters,* ***69***, p. 3098.

[17] Munz, M., Cappella, B., Sturm, H., Geuss, M., and Schulz, E., 2003. "Materials contrasts and nanolithography techniques in scanning force microscopy (sfm) and their application to polymers and polymer composites". In *Filler-Reinforced Elastomers/Sanning Force Microscopy*, Vol. 164 of *Advances in Polymer Science*. Springer Berlin / Heidelberg, pp. 87–210. 10.1007/b11055.

[18] Wendel, M., Irmer, B., Cortes, J., Kaiser, R., Lorenz, H., Kotthaus, J., Lorke, A., and Williams, E., 1996. "Nanolithography with an atomic force microscope". *Superlattices and microstructures,* ***20***(3), pp. 349–356.

[19] Wiesauer, K., and Springholz, G., 2000. "Fabrication of semiconductor nanostructures by nanoindentation of photoresist layers using atomic force microscopy". *Journal of Applied Physics,* ***88***(12), DEC 15, pp. 7289–7297.

[20] Farin, G., 2002. *Curves and surfaces for CAGD: A practical guide. 5th ed.* USA: Morgan Kaufmann;.